Research on Optimization Scheduling of Microgrid Based on Multi-strategy Improved Chernobyl Disaster Optimization Algorithm

Xiaoge Wei, Yinlong Zhao*, Haowei Yao, and Hengjie Qin

Abstract—**To enhance the economic operation efficiency of microgrids and reduce pollutant emissions, this paper proposes an Improved Chernobyl Disaster Optimization algorithm (ICDO) to tackle the optimal scheduling problem of grid-connected microgrids. First, a grid-connected microgrid system encompassing photovoltaic generators, wind turbines, micro gas turbines, energy storage devices, and diesel generators is selected as the research object. The optimization objectives focus on minimizing the microgrid's economic operation cost, environmental protection cost, and total cost. A mathematical model for daily optimal scheduling of the microgrid is established, taking into account the microgrid's actual operational constraints, penalty costs for battery overcapacity, and load shedding. Subsequently, the basic Chernobyl Disaster Optimization (CDO) algorithm is enhanced by integrating tent chaotic mapping, a group cognitive mechanism, and a local search strategy. Following an analysis of the ICDO algorithm's time complexity, ten standard test functions are utilized for ablation studies and performance evaluation. Simulation results illustrate the feasibility of the three proposed strategies and validate the effectiveness of the improved algorithm. Finally, the ICDO algorithm is applied alongside PSO, GWO, DBO, and CDO algorithms to solve the microgrid's daily optimal scheduling model. The results show that regardless of whether the objective function is economic operation cost, environmental protection cost, or total cost, the ICDO algorithm demonstrates significant advantages. This effective optimization approach substantially reduces the microgrid's economic operation expenses and environmental protection costs.**

Index Terms—**microgrid, optimal dispatch, CDO algorithm, group cognition mechanism, local search.**

Manuscript received March 19, 2025; revised June 23, 2025.

This work was supported by Henan Province Key R&D Special Project (Grant No.: 231111322200), the Henan province Central guidance local science and technology development fund project (Grant No.: Z20231811020), the Science and Technology Research Plan of Henan Province (Grant No.: 242102321033, 242102241051, 242102321104)

Xiaoge Wei is an associate professor in the School of Built Environment Engineering, Zhengzhou University of Light Industry, Zhengzhou, 450001, China. (e-mail: weixiaoge@zzuli.edu.cn)

Yinlong Zhao is a postgraduate student of the School of Building Environment Engineering, Zhengzhou University of Light Industry, Zhengzhou, China. (corresponding author to provide e-mail: 332222030896@email.zzuli.edu.cn)

Haowei Yao is an associate professor in the School of Built Environment Engineering, Zhengzhou University of Light Industry, Zhengzhou, China. (e-mail: yaohaowei@zzuli.edu.cn)

Hengjie Qin is an associate professor in the School of Built Environment Engineering, Zhengzhou University of Light Industry, Zhengzhou, China. (e-mail: qhj102432@zzuli.edu.cn)

I. INTRODUCTION

THE primary source of energy used in traditional power systems is the fossil fuels, which poses serious environmental pollution issues as well as resource depletion and climate change [1]. Therefore, people prefer clean energy sources such as solar and wind power to meet electricity demand and environmental sustainability requirements [2]. In this context, microgrids have emerged as a viable solution. Microgrids employ clean energy sources like solar and wind power through distributed generators, which to some extent reduces dependence on fossil fuels, promotes energy transition, decreases carbon emissions, and improves environmental quality. However, solar and wind power are significantly affected by weather conditions, thereby impacting the consistent operation of microgrids [3]. Meanwhile, compared to the traditional power grids, the microgrids have complex structures (involving wind power, solar power, energy storage, micro gas turbines, diesel generators, etc.), which increases the difficulty of coordinated scheduling [4]. Therefore, microgrid optimization scheduling is crucial to ensuring the steady and effective operation of microgrids.

A. Literature Review

The core concept underpinning microgrid optimization scheduling is the efficient allocation of output and operational hours across dispersed units to minimize environmental impact and operational expenses, all while ensuring a balanced power supply and adhering to various constraints [5]. Owing to the nonlinear, multi-constrained, and non-convex characteristics of microgrid optimization scheduling, an intelligent algorithm is necessitated [6], [7]. In past research, it has been identified that algorithms including Particle Swarm Optimization [8], [9], Genetic Algorithm [10], Sparrow Search Algorithm [11], Farm Land Fertility Algorithm [12], Differential Evolution [13], Grey Wolf Optimizer [14], Whale Optimization Algorithm [15], Salp Swarm Algorithm [16], Slime Mould Algorithm [17], and Hybrid Algorithms [18], among others, have been applied to address microgrid optimization issues. While the standard Particle Swarm Optimization algorithm benefits from structural simplicity and low parametric demands, it is prone to premature convergence and suboptimal solutions. Roy *et al.* [8] accomplished the optimal scheduling of a grid-connected microgrid over a 24-hour period by utilizing a particle swarm optimization algorithm integrated with a weighted aggregation approach. Zhang *et al.* [9] developed a

multi-objective particle swarm optimization technique to maximize service dependability while reducing operational costs and expenses associated with environmental protection. Despite their parallel evolutionary architecture and adaptive learning capacity, Genetic Algorithms face programming complexity and slow convergence limitations. Askarzadeh *et al.* [10] proposed a memory-based genetic algorithm for solving the minimum cost operation scheduling of microgrids. While the Sparrow Search Algorithm exhibits superior global exploration capacity, it is susceptible to premature convergence. Nguyen *et al.* [11] presented a sparrow search algorithm that optimizes microgrid operating plans by combining elite reverse learning and the firefly method's mutation technique. The farmland fertility algorithm is a nature-inspired metaheuristic algorithm, but it also suffers from slow convergence and an imbalance between global search and local exploitation capabilities. Mandloi *et al.* [12] presented an agricultural fertility algorithm to address microgrid and overall economic dispatch issues. The differential evolution algorithm is simple and efficient but easily falls into local optima and performs poorly on high-dimensional problems. Kamal *et al.* [13] developed a microgrid model for rural areas, which employs a differential evolution algorithm to compute the minimum energy cost and identify feasible component configurations. When it comes to microgrid optimization scheduling challenges, the conventional grey wolf optimizer has the problem of quickly becoming trapped in local optima, which leads to poor scheduling schemes. Liu *et al.*'s [14] introduced the Levy flight strategy, mutation strategy, and chaos strategy to address the drawbacks of the grey wolf algorithm in microgrid optimal scheduling. The basic Whale Optimization Algorithm is simple with few parameters but converges slowly, has low accuracy, and risks local optima. Zhang *et al.* [15] solved the issue of classic Whale Optimization Algorithms slipping into local optima in microgrid optimization scheduling by including reverse learning and nonlinear variable components into the fundamental algorithm. The Salp Swarm Algorithm is simple to operate and has few parameters, but it may fail to find the optimal solution in the later iterations. Belboul *et al.* [16] suggested an enhanced Salp Swarm method for solving the microgrid optimization scheduling problem. For complicated problems, the Slime Mould Algorithm may converge slowly and settle into local optima, despite its excellent exploration and exploitation capabilities. Behera *et al.* [17] solved the microgrid optimization scheduling issue using the slime mold method for the first time, with the goal of lowering emissions and operating costs. Although hybrid algorithms increase algorithm complexity and parameter adjustment difficulties, they integrate the advantages of many techniques to improve solution quality and robustness. Bektas *et al.* [18] solved microgrid optimization management difficulties by combining the simulated annealing approach and genetic algorithm while taking geographical circumstances and constraint variables into account.

Although researchers have made many advancements in the field of microgrid optimization scheduling algorithms, there is still great potential for optimization due to the complexity of the constraints. In light of this, this paper introduces an algorithm——the Chernobyl Disaster Optimization Algorithm (CDO). The CDO algorithm [19], proposed by Hisham A. Shehadeh, is a new metaheuristic optimization algorithm mainly inspired by the explosion of the Chernobyl nuclear reactor core. Its advantages include efficient search capability, ease of escaping local optima, and the potential to handle tasks across multiple domains. However, the CDO algorithm has difficulties including inadequate population diversity and constrained optimization capabilities while handling multi-constrained optimization issues. With the goal of offering a more efficient solution for microgrid optimization scheduling, this paper suggests an enhanced ICDO algorithm based on tent chaotic mapping, swarm cognitive mechanism, and local search strategy in response to the aforementioned problems.

B. Research Contribution

The primary research contributions of this paper are as follows:

(1) A model of a grid-connected microgrid system including energy storage devices, diesel generators, micro-gas turbines, wind, and solar electricity has been built.

(2) An ICDO algorithm is proposed, which is improved through the integration of tent chaotic mapping, swarm cognitive mechanism, and a refined local search strategy, thereby enhancing its global search and local exploitation capabilities.

(3) To confirm the viability of the three suggested methodologies and the efficacy of the enhanced algorithm, the ICDO algorithm's performance was tested and ablation research was carried out using ten standard test functions with thirty dimensions.

(4) The usefulness of the algorithm's improvements and the viability of the built model were both successfully confirmed by applying the enhanced ICDO algorithm, along with other algorithms, to the microgrid optimal scheduling model.

The paper is structured as follows. Section 2 presents the microgrid optimal scheduling model. Section 3 delves into the fundamental principles of the CDO algorithm. Section 4 elaborates on the improvement strategies employed in the ICDO algorithm. Section 5 showcases the comprehensive performance assessment of the proposed algorithm. Section 6 contains a simulation-based analysis of a microgrid case study, and Section 7 deliberates on the key conclusions and research results.

II. MICROGRID OPTIMIZATION SCHEDULING MODEL

This paper investigates a microgrid encompassing diverse distributed energy units, with photovoltaic power generation systems (PV), wind power generation systems (WT), micro gas turbines (MT), diesel power generation systems (DE), and batteries for energy storage (BESS). The microgrid is interconnected with the main grid (GRID) through a public connection point (PCC).

A. Objective function

The microgrid in this article operates in a grid-connected mode, and its total cost consists of two parts: economic operation cost and environmental protection cost.

(1) Economic operation cost of the microgrid

The operational costs of the microgrid in grid-connected

mode consist of the operation and maintenance costs as well as fuel expenses for both DE and MT, the maintenance costs of BESS, the cost of grid interaction, and penalty fees. The operational cost function is formulated as:

$$\begin{cases} f_1 = \sum_{t=1}^{24} (C_{MT}(t) + F_{DE}(t) + C_{OM}(t) + C_{GRID}(t) + C_{punish}) \\ C_{OM}(t) = k_{MT} P_{MT}(t) + k_{DE} P_{DE}(t) + k_{BESS} P_{BESS}(t) \\ C_{GRID}(t) = C_{buy}(t) P_{buy}(t) - C_{sell}(t) P_{sell}(t) \end{cases} \quad (1)$$

Here, $C_{MT}(t)$ denotes the fuel cost of the MT at time t. F_{DE} signifies the fuel cost of the diesel generator. $C_{OM}(t)$ denotes the operation and maintenance cost of distributed energy sources at time t, while $C_{GRID}(t)$ signifies the grid interaction cost at time t. P_{MT}, P_{DE}, and P_{BESS} respectively denote the output power of the MT, DE, and BESS at time t. k_{MT}, k_{DE}, and k_{BESS} respectively represent the operation and maintenance coefficients of MT, DE, and BESS. $C_{buy}(t)$ and $C_{sell}(t)$ denote the purchasing and selling electricity prices at time t. $P_{buy}(t)$ and $P_{sell}(t)$ indicating the purchasing and selling electricity power at time t.

The penalty cost C_{punish} for load loss and battery overcharging is as follows:

$$C_{punish} = \alpha_{punish} P_{loss}(t) + \beta_{punish} P_{over}(t) \quad (2)$$

Here, α_{punish} and β_{punish} represents the load loss and battery overcapacity penalty coefficients respectively. $P_{loss}(t)$ denotes the load loss at time t, and $P_{over}(t)$ indicates the excess capacity of the battery at time t.

(2) Microgrid grid-connected environmental protection costs

During the operation of the MT, DE, and grid interaction, the k-th type of pollutant produced (when k=1, the pollutant is CO2; when k=2, the pollutant is SO2; when k=3, the pollutant is NOx). Thus, when a microgrid operates in grid - connected mode, its environmental protection costs denote the expenditures for handling the k - th type of pollutant, specified as below.

$$\begin{cases} f_2 = \sum_{t=24}^{T} (C_{MT.EN}(t) + C_{DE.EN}(t) + C_{GRID.EN}(t)) \\ C_{MT.EN}(t) = \sum_{k=1}^{3} (C_k \gamma_{MT,k}) P_{MT}(t) \\ C_{DE.EN}(t) = \sum_{k=1}^{3} (C_k \gamma_{DE,k}) P_{DE}(t) \\ C_{GRID.EN}(t) = \sum_{k=1}^{3} (C_k \gamma_{GRID,k}) P_{buy}(t) \end{cases} \quad (3)$$

Here, $C_{MT.EN}(t)$, $C_{DE.EN}(t)$, and $C_{GRID.EN}(t)$ denote the pollutant treatment costs of the MT, DE, and the main grid respectively. $\gamma_{MT,k}$, $\gamma_{DE,k}$, and $\gamma_{GRID,k}$ signify the discharges of the k-th pollutant category emitted by the MT, DE, and the primary power grid respectively. C_k denotes the cost coefficient of treating the k-th type of pollutant.

(3) Total cost objective function of the microgrid

The total cost of the microgrid includes not only the operating cost f_1, but also the environmental protection cost f_2. Therefore, the total cost Z is defined as Equation (4), and minimized the total cost Z serves as the objective.

$$Z = \min(f_1 + f_2) \quad (4)$$

B. Constraints

For the optimal scheduling of the microgrid in grid-connected mode, the constraints are described as follows:

(1) Power balance constraint

$$P_{PV}(t) + P_{WT}(t) + P_{GRID}(t) + P_{DE}(t) + P_{MT}(t) + P_{BESS}(t) = P_L(t) \quad (5)$$

(2) Diesel generator output constraints

$$\begin{cases} P_{DE}^{\min}(t) \le P_{DE}(t) \le P_{DE}^{\max}(t) \\ \left| P_{DE}(t) - P_{DE}(t-1) \right| \le r_{DE} \end{cases} \quad (6)$$

(3) Micro gas turbine output constraints

$$\begin{cases} P_{MT}^{\min}(t) \le P_{MT}(t) \le P_{MT}^{\max}(t) \\ \left| P_{MT}(t) - P_{MT}(t-1) \right| \le r_{MT} \end{cases} \quad (7)$$

(4) Contact line constraints

$$P_{GRID}^{\min}(t) \le P_{GRID}(t) \le P_{GRID}^{\max}(t) \quad (8)$$

(5) Energy storage device constraints

$$\begin{cases} P_{BESS}^{\min}(t) \le P_{BESS}(t) \le P_{BESS}^{\max}(t) \\ SOC^{\min}(t) \le SOC(t) \le SOC^{\max}(t) \end{cases} \quad (9)$$

Here, P_{PV} denotes the actual output power of the photovoltaic cell, while P_{WT} represents the output power of the WT. The variable $P_L(t)$ signifies the microgrid load at time t. $P_{DE}^{\max}(t)$, $P_{DE}^{\min}(t)$, $P_{MT}^{\max}(t)$, and $P_{MT}^{\min}(t)$ respectively indicate the upper and lower bounds of the DE and MT output at time t. Similarly, r_{DE} and r_{MT} denote the maximum limits of the DE and MT power ramping rates. Additionally, $P_{GRID}^{\max}(t)$ and $P_{GRID}^{\min}(t)$ respectively stand for the upper and lower bounds of the tie line transmission power at time t. $P_{BESS}^{\max}(t)$ and $P_{BESS}^{\min}(t)$ define the upper and lower limits of the energy storage device's output at time t, while $SOC^{\max}(t)$ and $SOC^{\min}(t)$ specify the upper and lower limits of the energy storage capacity at time t.

III. Chernobyl Disaster Optimization Algorithm

The CDO algorithm simulates the process of nuclear radiation where α, β, and γ particles adhere to the human body after a nuclear explosion. Once the explosion occurs, these particles move away from the core carrier until they reach human settlements, triggering the disaster [19]. It is postulated that the individuals (humans) are in motion via walking when the particles are assaulting them. Assuming adults walk at speeds of 0-3 miles per hour outdoors within a circular walking area. Based on this, we can calculate the walking speed of individuals using Equation (10).

$$WS_{\mathrm{h}} = 3 - 1 * ((3) / Max\_iter) \quad (10)$$

$$x_{\mathrm{h}} = r^2 \cdot \pi \quad (11)$$

Here, WS_{h} represents the walking speed of individuals, linearly decreasing from 3 to 0. Max_iter refers to the upper limit of iteration counts for the algorithm, while x_{h} represents the area of the circular region surrounding the person while walking. In addition, r refers to the radius of the circle, which is a random value in the range from 0 to 1.

During the nuclear radiation process where α, β, and γ particles adhere to the human body, the gradient descent coefficients for the attack of these three particles on humans,

denoted as v_α, v_β, and v_γ, are as shown in Equation (12).

$$\begin{cases} v_\alpha = 0.25 \cdot (X_\alpha(t) - \rho_\alpha \cdot \Delta_\alpha) \\ v_\beta = 0.5 \cdot (X_\beta(t) - \rho_\beta \cdot \Delta_\beta) \\ v_\gamma = X_\gamma(t) - \rho_\gamma \cdot \Delta_\gamma \end{cases} \tag{12}$$

Here, $X_\alpha(t)$, $X_\beta(t)$, and $X_\gamma(t)$ denote the current positions of the α, β and γ particles, respectively. While ρ_α, ρ_β, and ρ_γ signify the propagation amounts of the α, β, and γ particles, respectively. Δ_α, Δ_β, and Δ_γ stand for the differences between the positions of the particles and the position of the person.

For the α, β, and γ particles, the update formulas for their propagation quantities are as follows:

$$\begin{cases} \rho_\alpha = \dfrac{x_h}{0.25 \cdot S_\alpha} - (WS_h \cdot rand()) \\ \rho_\beta = \dfrac{x_h}{0.5 \cdot S_\beta} - (WS_h \cdot rand()) \\ \rho_\gamma = \dfrac{x_h}{S_\gamma} - (WS_h \cdot rand()) \end{cases} \tag{13}$$

$$\begin{cases} S_\alpha = \log(rand(1:16000)) \\ S_\beta = \log(rand(1:270000)) \\ S_\beta = \log(rand(1:270000)) \end{cases} \tag{14}$$

Here, S_α, S_β, and S_γ represent the velocities of the α, β, and γ particles, respectively, which are normalized by taking their logarithms.

The formula for updating the distance between different particle positions and all particle positions is as follows:

$$\begin{cases} \Delta_\alpha = \left| A_\alpha \cdot X_\alpha(t) - X_T(t) \right| \\ \Delta_\beta = \left| A_\beta \cdot X_\beta(t) - X_T(t) \right| \\ \Delta_\gamma = \left| A_\gamma \cdot X_\gamma(t) - X_T(t) \right| \end{cases} \tag{15}$$

$$A_\alpha = A_\beta = A_\gamma = r^2 \cdot \pi \tag{16}$$

Here, A_α, A_β, and A_γ respectively represent the propagation areas of the α, β, and γ particles, which are the areas of circles with radius r($r \in (0,1)$). X_T denotes the positions of all particles.

Based on the gradient descent coefficients of α, β and γ particles, the updating formula for all particles is as follows:

$$X_T(t) = \frac{(v_\alpha + v_\beta + v_\gamma)}{3} \tag{17}$$

IV. Improvements to the Chernobyl Disaster Optimization Algorithm

This paper aims to address the issues of poor population diversity and optimization capabilities when solving multi-constrained optimization problems using the CDO Algorithm. Three improvement strategies are proposed as follows.

A. Population initialization - Tent Chaotic Mapping

For intelligent algorithms, population initialization constitutes a pivotal step [20]. The quality of population initialization exerts a direct influence on the algorithm's performance and search capabilities. The CDO algorithm initializes the population using random number methods, which have relatively weak randomness and traversal properties. This results in a non-uniform distribution of the generated population across the search space, causing the algorithm to be susceptible to local optima and restricting its global search performance. Tent chaotic mapping is a type of linear piecewise mapping [21] with a uniform distribution function and strong randomness. Therefore, tent chaotic mapping is applied for population initialization, contributing to the enhancement of population diversity. The specific calculation formula is described as follows.

$$x_{n+1} = \begin{cases} 2x_n & x_n \in [0, 0.5) \\ 2(1 - x_n) & x_n \in [0.5, 1] \end{cases} \tag{18}$$

$$y_i = x_i(ub - lb) + lb \tag{19}$$

Here, x_n and x_{n+1} denote the state variables prior to and after the tent chaotic mapping, respectively. The search region boundaries are represented by *ub* (upper bound) and *lb* (lower bound). y_i denotes the initial values of the particle population after applying the tent chaotic mapping.

B. Particle position update optimization - Particle Swarm Strategy

Within the traditional CDO algorithm, the position update equations of particles fail to comprehensively represent the optimal position information of particle α, resulting in inferior optimization performance in solving multi-constraint optimization issues. To overcome these problems, the group cognition mechanism of the particle swarm optimization algorithm is incorporated into the position update formula of all particles within the CDO algorithm [22]. The new individual position update strategy is presented as shown in Equation (20).

$$\begin{aligned} X_T(t) = \lambda \cdot rand() \cdot \frac{(v_\alpha + v_\beta + v_\gamma)}{3} + \\ (1 - \lambda) \cdot rand() \cdot (gbest_t - X_T(t)) \end{aligned} \tag{20}$$

In the formula, λ denotes the weight, which is set to 0.8 in this paper; rand is defined as a random number within the interval [0, 1]; $gbest_t$ represents the position of particle α at the t-th iteration of the algorithm.

C. Local search strategy - Hill Climbing

In response to the issue of poor optimization capability of the traditional CDO algorithm under multiple constraints, this paper introduces a local search strategy to optimize and improve it. Hill climbing, as an efficient local search algorithm [23], operates by starting from the current solution, evaluating and selecting a better neighboring solution, and repeating this process until a termination condition is met. Aiming to improve the CDO algorithm's local search proficiency and help it break free from local optima, this study performs a local search on the determined global optimal location after each iteration cycle. The following are the precise steps for implementation.

(1) The global optimal position obtained in each iteration cycle of the CDO algorithm is used as the starting solution of the hill climbing algorithm.

(2) A set of neighboring solutions around the starting solution are generated to ensure that these solutions are within the search space.

(3) The fitness values of the initial solution and its adjacent solutions are assessed, and the solution with the best fitness is

chosen as the new solution according to the greedy principle.

(4) Check whether the termination condition (usually the dimensionality of the solution) is met. If the condition is satisfied, the loop ends. In the absence of satisfaction, the loop runs repeatedly until the condition is met.

D. The flowchart of the ICDO algorithm

Given the issues encountered in the CDO algorithm when solving multi-constraint problems, multiple strategies are integrated to improve it in this paper. The enhanced flowchart of the ICDO is depicted in Figure 1.

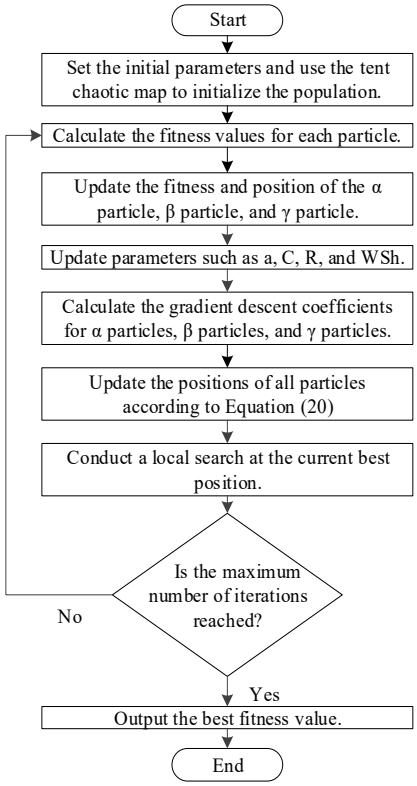

Fig. 1. The flow chart of the ICDO algorithm

The detailed procedures of the enhanced ICDO algorithm are outlined as follows:

Step 1: Utilize the Tent Chaotic Map to initialize the population and configure the corresponding parameters.

Step 2: Compute the fitness value for each particle, and then update the fitness values and positions of the α, β, and γ particles.

Step3: Update a, C, R, WSh and other related parameters.

Step4: Calculate the gradient descent coefficients of α, β and γ particles according to Equation (12).

Step 5: Integrate the group cognition mechanism into the position update formula for all particles, and utilize the revised Equation (20) to update their positions.

Step6: Carry out local search of the current best fitness value and optimal location by mountain climbing method.

Step 7: Check if the maximum number of iterations has been reached. If not, return to Step 2.

Step8: Output the optimal fitness value and optimal position.

E. Time complexity analysis

Assuming that the population size is represented by N, the dimensionality of each individual is n, the time for parameter initialization is represented as t_0, the time required for initializing each dimension of the particle population is t_1, the time for calculating the fitness value of each particle is $f(n)$, and the time for determining the three types of particles based on fitness values is t_2, then the complexity of the CDO algorithm in terms of time during the phase of initializing the population is as follows:

$$T_1 = o(t_0 + N \cdot (n \cdot t_1 + f(n)) + t_2) = o(n + f(n)) \quad (21)$$

After entering the loop iteration, the number of iterations is set as Max_iter. For each iteration, the time taken to compute the walking speed WS_h of the person and the speed S of the particle is marked as t_3, the time taken to compute the spreading area A of the particle and the spreading amount ρ of the particle is labelde as t_4, the time taken to compute the distance between the positions of particles α, β, and γ and the human position according to Equation (15) is assigned as t_5, the time taken to compute the gradient descent coefficient according to Equation (12) is denoted by t_6, the time taken to calculate the positions of all particles according to Equation (17) is denoted as t_7, the time required to handle the boundary of each dimension of the particle individual is designated as t_8, the time taken to compute the individual fitness value remains $f(n)$, and the time required to update particles α, β, and γ is termed t_9. Therefore, the time complexity within a single loop is:

$$\begin{aligned} T_2 &= o(N \cdot (t_3 + t_4 + 3 \cdot (t_5 + t_6) + t_7) + n \cdot t_8 + f(n) + t_9) \\ &= o(n + f(n)) \end{aligned} \quad (22)$$

Thus, the overall time complexity of the CDO algorithm can be described as:

$$T = T_1 + Max\_iter \cdot T_2 = o(n + f(n)) \quad (23)$$

In the ICDO algorithm, the population size is represented by N, where each individual possesses a dimension of n. During the population initialization phase, the tent chaotic mapping approach is utilized for initialization. The time taken for the tent chaotic mapping strategy is represented as d1, while other parameters remain consistent with those in the CDO algorithm. Therefore, the time complexity of the ICDO algorithm in the initialization phase can be stated as follows:

$$\begin{aligned} T_3 &= o(t_0 + N \cdot (n \cdot t_1 + n \cdot d_1 + f(n)) + t_2) \\ &= o(n + f(n)) \end{aligned} \quad (24)$$

In a single iteration, the main difference between the ICDO algorithm and the CDO algorithm lies in the optimization of particle position updating and the introduction of a local search strategy. For the optimization of particle position, the group cognition mechanism is directly incorporated into all particle position update formulas without additional computational steps. Therefore, the time taken to calculate the positions of all the particles is still t_7. According to the local search strategy of the hill climbing method, the time taken to compute the optimal position of the particle population is c_1. Thus, the time complexity of this stage is:

$$\begin{aligned} T_4 &= o(N \cdot (t_3 + t_4 + 3 \cdot (t_5 + t_6) + t_7) + n \cdot (t_8 + c_1) + f(n) + t_9) \\ &= o(n + f(n)) \end{aligned} \quad (25)$$

Therefore, the aggregate time complexity of the ICDO algorithm is:

$$T' = T_3 + Max\_iter \cdot T_4 = o(n + f(n)) \quad (26)$$

In conclusion, the optimization of the ICDO algorithm in

this paper does not change its temporal complexity, which remains consistent with that of the original CDO algorithm.

V. Optimization Achievement Test of the ICDO Algorithm

To assess the performance of the ICDO algorithm, ten internationally recognized standard benchmark test functions were chosen. Initially, ablation studies were carried out to separately confirm the efficacy of the three core strategies incorporated into the CDO algorithm framework. Following this, the ICDO algorithm was evaluated for its convergence and optimization precision to demonstrate the efficiency of the enhanced algorithm.

A. Introduction to standard test functions

This paper evaluates the performance of the ICDO algorithm using 10 internationally acknowledged test function sets. Specifically, F_1 to F_5 represent unimodal functions, while F_6 to F_{10} correspond to multimodal functions, as detailed in Table 1. To guarantee the reliability and fairness of the experimental outcomes, the population size N for all comparison algorithms is uniformly set to 30, with a maximum iteration limit of 1000. Each algorithm is executed 50 times on each test function, and the mean, best value, and standard deviation of the results are recorded for each test group. The simulation environment consists of MATLAB R2018b as the software platform and Windows 10 as the operating system.

TABLE I
STANDARD TEST FUNCTION

Number	Function	Variable value range S	Optimal value F
Unimodal test function			
F_1	Sphere	$[-100;100]^n$	0
F_2	Schwefel's Problem 2.22	$[-10;10]^n$	0
F_3	Schwefel's Problem 1.2	$[-100;100]^n$	0
F_4	Schwefel's Problem 2.21	$[-100;100]^n$	0
F_5	Quartic Function i.e. Noise	$[-1.28;1.28]^n$	0
Multimodal test function			
F_6	Generalized Rastrigin's Function	$[-5.12;5.12]^n$	0
F_7	Ackley's Function	$[-32;32]^n$	0
F_8	Generalized Griewank's Function	$[-600;600]^n$	0
F_9	Generalized Penalized Function 1	$[-50;50]^n$	0
F_{10}	Generalized Penalized Function 2	$[-50;50]^n$	0

B. Ablation research

To validate the efficacy of the three proposed strategies, based on the above standard test functions, comparative tests were conducted sequentially on five intelligent algorithms: the basic Chernobyl Disaster Optimization (CDO), the Chernobyl Disaster Optimization algorithm integrated with Tent chaotic mapping (TCDO), the Chernobyl Disaster Optimization algorithm integrated with group cognitive mechanism (PCDO), the Chernobyl Disaster Optimization algorithm integrated with local search strategy (LCDO), and the ICDO algorithm. The results are summarized in Table 2.

TABLE II
COMPARISON RESULTS OF ABLATION STUDIES

function	algorithm	d=30		
		Optimal value	Mean value	standard deviation
F_1	CDO	2.22E-273	5.64E-260	0.00E+00
	TCDO	3.26E-272	2.31E-260	0.00E+00
	PCDO	0.00E+00	0.00E+00	0.00E+00
	LCDO	8.79E-275	3.27E-264	0.00E+00
	ICDO	0.00E+00	0.00E+00	0.00E+00
F_2	CDO	1.82E-138	5.71E-133	2.21E-132
	TCDO	9.99E-139	1.83E-133	6.51E-133
	PCDO	0.00E+00	0.00E+00	0.00E+00
	LCDO	1.32E-139	1.87E-135	4.33E-135
	ICDO	0.00E+00	0.00E+00	0.00E+00
F_3	CDO	1.29E-242	9.40E-200	0.00E+00
	TCDO	3.99E-246	1.33E-197	0.00E+00
	PCDO	0.00E+00	0.00E+00	0.00E+00
	LCDO	1.50E-247	2.11E-205	0.00E+00
	ICDO	0.00E+00	0.00E+00	0.00E+00
F_4	CDO	8.47E-129	2.07E-121	1.35E-120
	TCDO	1.03E-130	4.45E-122	1.78E-121
	PCDO	0.00E+00	0.00E+00	0.00E+00
	LCDO	9.29E-131	2.15E-122	1.02E-121
	ICDO	0.00E+00	0.00E+00	0.00E+00
F_5	CDO	5.00E-06	7.45E-05	6.49E-05
	TCDO	5.24E-07	7.83E-05	5.90E-05
	PCDO	2.62E-06	3.56E-05	3.60E-05
	LCDO	1.67E-06	6.44E-05	5.75E-05
	ICDO	3.01E-07	3.68E-05	4.06E-05
F_6	CDO	0.00E+00	1.28E+02	1.05E+02
	TCDO	0.00E+00	1.42E+02	1.01E+02
	PCDO	0.00E+00	0.00E+00	0.00E+00
	LCDO	0.00E+00	2.02E-01	1.93E-01
	ICDO	0.00E+00	0.00E+00	0.00E+00
F_7	CDO	4.44E-15	4.44E-15	2.37E-30
	TCDO	4.44E-15	4.44E-15	1.58E-30
	PCDO	8.88E-16	8.88E-16	9.86E-32
	LCDO	4.44E-15	4.44E-15	1.58E-30
	ICDO	8.88E-16	8.88E-16	9.86E-32
F_8	CDO	0.00E+00	3.79E-03	8.52E-03
	TCDO	0.00E+00	3.89E-03	5.13E-03
	PCDO	0.00E+00	0.00E+00	0.00E+00
	LCDO	0.00E+00	3.66E-03	5.73E-03
	ICDO	0.00E+00	0.00E+00	0.00E+00
F_9	CDO	1.11E+00	1.27E+00	2.58E-01
	TCDO	1.11E+00	1.20E+00	2.10E-01
	PCDO	1.67E+00	1.67E+00	2.81E-04
	LCDO	7.82E-04	3.01E-03	2.04E-03
	ICDO	2.71E-04	3.13E-03	3.99E-03
F_{10}	CDO	3.13E-01	4.22E-01	7.78E-02
	TCDO	2.73E-01	4.14E-01	7.97E-02
	PCDO	1.48E+00	1.89E+00	1.86E-01
	LCDO	2.12E-03	2.52E-02	1.16E-02
	ICDO	6.48E-03	2.77E-02	1.30E-02

The following inferences can be derived from Table 2:

For the TCDO algorithm, its performance on functions F_2, F_4, F_7, F_9, and F_{10} is remarkably superior to that of the CDO algorithm. On function F_1, while the optimal value of the TCDO algorithm is marginally less than that of the CDO algorithm by an order of magnitude, it surpasses the CDO algorithm in terms of average value and standard deviation. On functions F_3, F_5, F_6, and F_8, the average values of the TCDO algorithm and the CDO algorithm are within the same order of magnitude, and the TCDO algorithm still retains advantages in terms of standard deviation and optimal value, which confirms the effectiveness of the Tent chaotic mapping population initialization strategy.

For the PCDO algorithm, although its performance on functions F_9 and F_{10} is not as good as that of the CDO algorithm, its optimal values, average values, and standard

deviations on functions F_1~F_8 are all superior to those of the CDO algorithm, proving the feasibility of integrating the group cognitive mechanism.

For the LCDO algorithm, on functions F_1~F_{10}, it surpasses the CDO algorithm in terms of optimal value, average value, and standard deviation, which validates the effectiveness of incorporating the local search strategy.

In summary, the findings of the ablation study indicate that the ICDO algorithm exhibits remarkably superior performance compared to the other four benchmark algorithms across the 10 standard test functions. Moreover, the TCDO, PCDO, and LCDO algorithms all outperform the CDO algorithm, thereby confirming that the three optimization strategies effectively improve the search performance of the CDO algorithm.

C. Optimization Accuracy and Convergence Analysis

Based on the above ten standard test functions, a comparative analysis of the optimization accuracy and convergence of the PSO [24], GWO [25], DBO [26], CDO [19], and ICDO algorithms was conducted. The parameter configurations of each algorithm are presented in Table 3.

TABLE III
PARAMETER SETTINGS

Algorithm	Parameter
PSO	Inertia weight ω =0.9, V_{max}=2, V_{min}=-2, C_1=C_2=2
GWO	Control parameter a_{max} = 2， a_{min} = 0
DBO	K and λ=0.1, b=0.3, S=0.5
CDO ICDO	S_α= rand (1,16000), S_β= rand (1,27000), S_γ=rand (1,300000), r = rand (0,1)

After multiple repeated experiments, the average value, optimal value, and standard deviation of the PSO, GWO, DBO, CDO, and ICDO algorithms were recorded. The results are presented in Table 4 as follows.

(1) Table 4 indicates the following:

1) For functions F_1 to F_4, the ICDO algorithm attains an optimal solution of 0 across the average value, optimal value, and standard deviation, surpassing the other four comparative algorithms. For function F_5, although the ICDO algorithm fails to achieve the optimal solution in terms of the average value, optimal value, and standard deviation, it still demonstrates superior performance over the other four algorithms.

2) For functions F_6, F_7, and F_{10}, the ICDO algorithm outperforms the other four comparative algorithms in terms of optimal value, average, and standard deviation. For functions F_8, the CDO, GWO, DBO, and ICDO algorithms all reach the optimal value of 0, exceeding the PSO algorithm. Additionally, the ICDO and DBO algorithm attain the optimal solution for the average value and standard deviation, outperforming the other three comparative algorithms. For function F_9, while the ICDO algorithm shows a marginal performance deficit compared to the DBO algorithm in terms of optimal value and average, it exhibits stronger robustness and is significantly superior to the other three comparative algorithms.

(2) To more intuitively compare the overall improvement performance of the optimization algorithms, Figure 2 presents the convergence curves of the five algorithms for various test functions.

TABLE IV
PERFORMANCE COMPARISON AMONG DIFFERENT ALGORITHMS

function	algorithm	d=30		
		Optimal value	Mean value	standard deviation
F_1	CDO	2.22E-273	5.64E-260	0.00E+00
	ICDO	0.00E+00	0.00E+00	0.00E+00
	GWO	2.68E-62	5.47E-59	1.22E-58
	PSO	8.95E-02	1.81E-01	5.45E-02
	DBO	1.64E-306	3.17E-207	0.00E+00
F_2	CDO	1.82E-138	5.71E-133	2.21E-132
	ICDO	0.00E+00	0.00E+00	0.00E+00
	GWO	1.13E-35	1.37E-34	1.87E-34
	PSO	1.09E+00	2.66E+00	1.08E+00
	DBO	4.16E-158	3.59E-123	2.47E-122
F_3	CDO	1.29E-242	9.40E-200	0.00E+00
	ICDO	0.00E+00	0.00E+00	0.00E+00
	GWO	3.48E-21	1.62E-14	7.96E-14
	PSO	4.40E+00	1.45E+01	4.42E+00
	DBO	4.97E-302	3.04E-88	2.13E-87
F_4	CDO	8.47E-129	2.07E-121	1.35E-120
	ICDO	0.00E+00	0.00E+00	0.00E+00
	GWO	6.96E-16	1.67E-14	1.89E-14
	PSO	5.71E-01	1.82E+00	1.20E+00
	DBO	1.71E-152	2.15E-111	1.34E-110
F_5	CDO	5.00E-06	7.45E-05	6.49E-05
	ICDO	3.01E-07	3.68E-05	4.06E-05
	GWO	1.97E-04	7.68E-04	3.17E-04
	PSO	9.27E-03	5.14E-02	2.93E-02
	DBO	2.76E-05	7.14E-04	5.83E-04
F_6	CDO	0.00E+00	1.28E+02	1.05E+02
	ICDO	0.00E+00	0.00E+00	0.00E+00
	GWO	0.00E+00	2.37E-01	1.19E+00
	PSO	4.68E+01	7.39E+01	1.31E+01
	DBO	0.00E+00	1.19E-01	8.36E-01
F_7	CDO	4.44E-15	4.44E-15	2.37E-30
	ICDO	8.88E-16	8.88E-16	9.86E-32
	GWO	2.37E-01	1.59E-14	2.95E-15
	PSO	7.39E+01	2.29E+00	6.38E-01
	DBO	8.88E-16	9.59E-16	4.97E-16
F_8	CDO	0.00E+00	3.79E-03	8.52E-03
	ICDO	0.00E+00	0.00E+00	0.00E+00
	GWO	0.00E+00	6.37E-04	2.60E-03
	PSO	1.69E-02	5.23E-02	1.89E-02
	DBO	0.00E+00	0.00E+00	0.00E+00
F_9	CDO	1.11E+00	1.27E+00	2.58E-01
	ICDO	2.71E-04	3.13E-03	3.99E-03
	GWO	6.54E-03	3.78E-02	2.64E-02
	PSO	2.76E-02	3.38E+00	1.65E+00
	DBO	2.92E-13	2.07E-03	1.45E-02
F_{10}	CDO	3.13E-01	4.22E-01	7.78E-02
	ICDO	6.48E-03	2.77E-02	1.30E-02
	GWO	2.03E-01	5.14E-01	1.48E-01
	PSO	3.08E-02	1.04E-01	4.77E-02
	DBO	1.10E-02	2.97E-01	2.35E-01

As illustrated in Figure 2, the ICDO algorithm surpasses the GWO, PSO, DBO, and CDO algorithms in terms of convergence speed and optimization capability. For functions F_1 through F_4 and F_6 through F_8, the ICDO algorithm exhibits substantial improvements in both convergence speed and optimization capability, clearly outmatching the other algorithms. In function F_5 and F_{10}, while the ICDO algorithm does encounter local optima, it manages to escape them more swiftly than its counterparts, and it achieves a significantly superior optimal value. In function F_9, although the ICDO algorithm's convergence speed lags slightly behind PSO, it is still ahead of GWO, DBO, and CDO, and it demonstrates formidable optimization capabilities.

In summary, the ICDO algorithm consistently demonstrates a faster convergence speed, good stability, and strong global search capabilities, validating the effectiveness

of the proposed improvements.

VI. Case Paper Analysis

A. Case parameters

In this paper, the microgrid grid-connected model mentioned earlier is utilized as a case paper. The chosen distributed units consist of PV, WT, DE, MT, and the energy storage device BESS. The energy storage equipment boasts a maximum capacity of 150kWh, a minimum capacity of 5kWh, an initial capacity of 50kWh, and both its maximum output and input power are capped at 30kW, featuring a

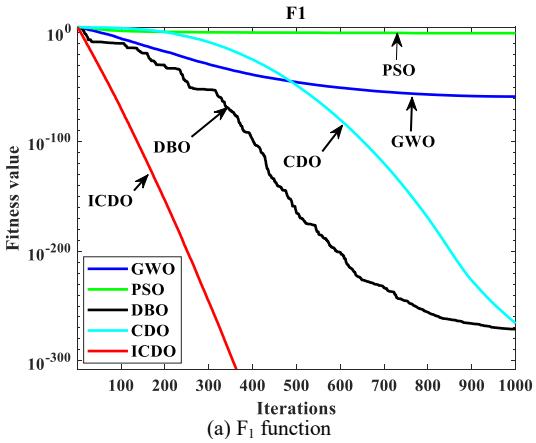

(a) F_1 function

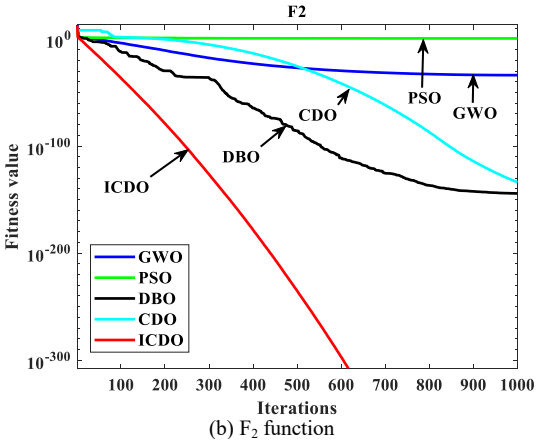

(b) F_2 function

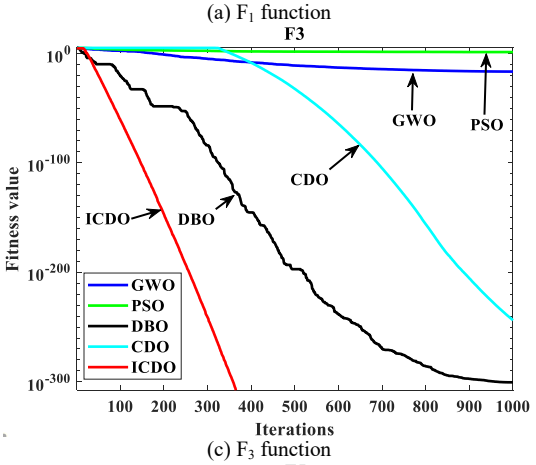

(c) F_3 function

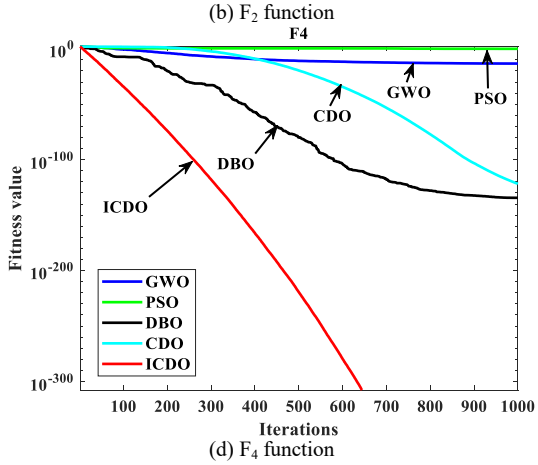

(d) F_4 function

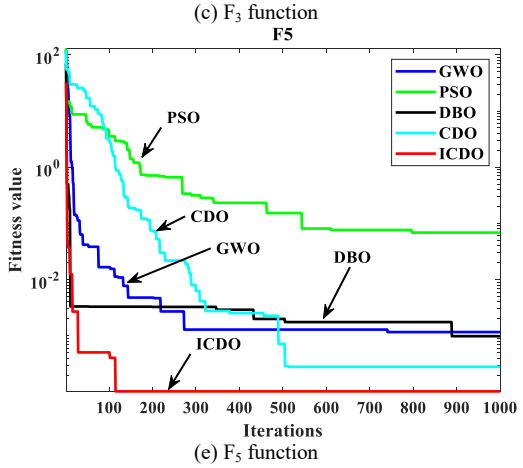

(e) F_5 function

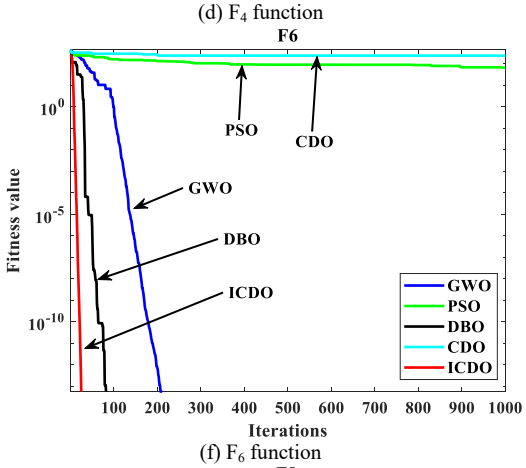

(f) F_6 function

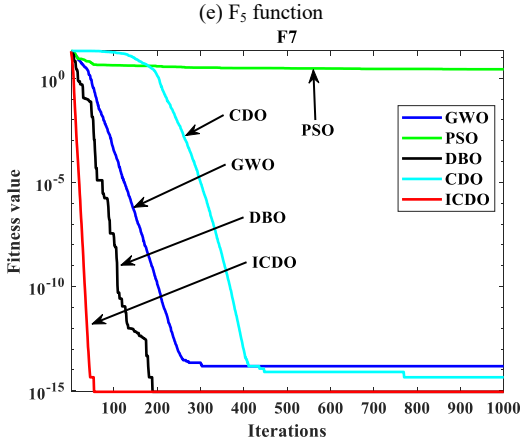

(g) F_7 function

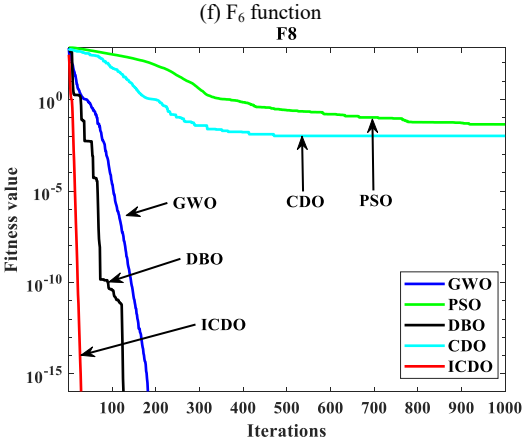

(h) F_8 function

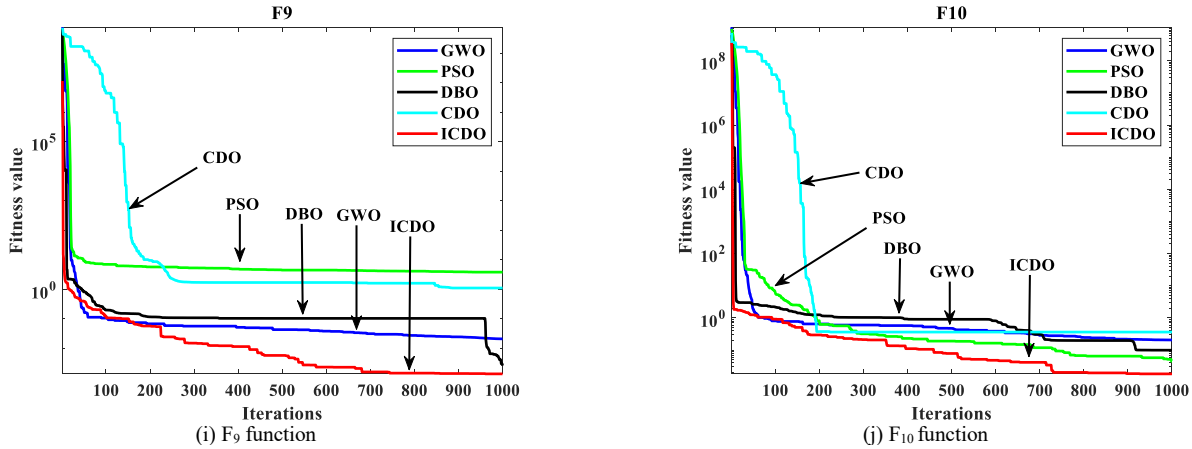

(i) F_9 function (j) F_{10} function

Fig. 2. The convergence curves of various test functions

charge-discharge efficiency of 0.9. The parameters for these units are listed in Table 5 [27], while the emission coefficients of pollutants and the associated costs of pollution treatment are detailed in Table 6 [27]. The time-of-use electricity price parameters adopted in this paper are listed in Table 7 [28]. The forecast data of wind power, photovoltaic and load in a certain place are shown in Figure 3.

TABLE V
UNIT PARAMETERS OF EACH DISTRIBUTED UNIT

Power type	Power upper limit /kW	Power lower limit /kW	Operating and maintenance unit price / (yuan/ *kW•h*)	Ramping upper power limit (kW/min)
PV	50	0	0	0
WT	100	0	0	0
MT	30	3	0.0293	1.5
DE	65	0	0.04	1.5
GRID	30	-30	0	0

TABLE VI
POLLUTANT PROTECTION COST AND EMISSION COEFFICIENT

Type	Treatment cost/ (yuan/Kg)	Emission coefficient of pollutants / (g/ *kW•h*)		
		DE	GRID	MT
CO_2	0.023	680	889	724
SO_2	6	0.306	1.8	0.0036
NO_x	8	10.09	1.6	0.2

TABLE VII
TIME-OF-USE ELECTRICITY PRICE PARAMETERS

Type	Corresponding time period	Electricity purchase price (yuan/kWh)	Electricity sales price (yuan/kWh)
Peak time	10:00--15:00 18:00--22:00	0.86	0.5
Level time	08:00--09:00 16:00--17:00	0.54	0.5
Valley time	01:00--07:00 23:00--24:00	0.32	0.5

B. Simulation results analysis

Utilizing day-ahead forecasting data for loads, wind turbines, and photovoltaic systems from practical engineering scenarios, this paper applies the ICDO, CDO, DBO, PSO, and GWO algorithms to solve the optimization scheduling model of a grid-connected microgrid system. The primary objectives are to minimize the economic operation cost, environmental protection cost, and comprehensive total cost, respectively. The algorithm parameters are set as a maximum iteration number of 300 and a population size of 100.

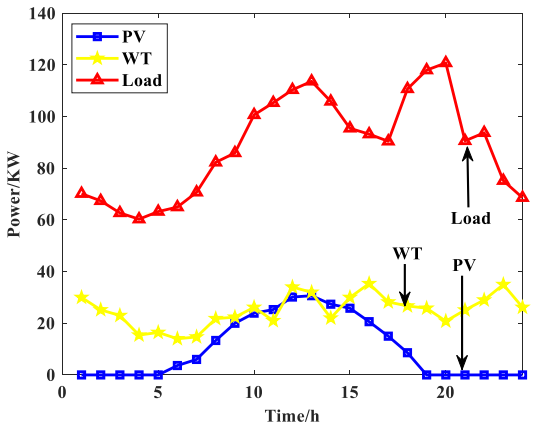

Fig. 3. Typical daily load, wind power forecast curve

(1) Algorithm comparison and analysis

1) Comparative analysis of the convergence of various algorithms

Figure 4 illustrates the iterative convergence curves of each algorithm for various objective functions. As illustrated in Figure 4, across various objective function scenarios, the ICDO algorithm demonstrates remarkable superiority over the other four comparative algorithms in both iterative convergence rate and optimization capability. In terms of local optima, between iterations 70 and 130, the CDO algorithm frequently falls into local optima traps, ultimately resulting in significantly less optimal solutions compared to PSO, GWO, DBO, and ICDO algorithms. PSO, GWO, and DBO algorithms rarely encounter the problem of falling into such traps during iterations, while the ICDO algorithm completely avoids them. In terms of convergence, PSO GWO, and DBO algorithms tend to stabilize around the 250th iteration, CDO around the 130th iteration, whereas the ICDO algorithm converges much faster, typically within 50 iterations. In terms of optimal solutions, the results derived by the ICDO algorithm through iterative cycles all outperform those of the PSO, GWO, DBO, and CDO algorithms, further verifying the superiority and effectiveness of the proposed ICDO algorithm.

2) Comparative Analysis of Optimization Results of Different Algorithms

To verify the improved effectiveness and stability of the optimized ICDO algorithm, each algorithm was run 30 times. As shown in Table 8, the comparative analysis uses the mean value, standard deviation, and minimum value of the results.

As evident from Table 8, when compared with the PSO, GWO, DBO, and CDO algorithms, the optimization capability and stability of the ICDO algorithm have been remarkably enhanced. Taking the minimum operating cost as the objective function for analysis, the ICDO algorithm significantly improves the solution efficiency of microgrid optimal scheduling, resulting in a reduction of the average cost by 14.62%, 9.22%, 23.12%, and 51.71% compared to the PSO, GWO, DBO, and CDO algorithms, respectively. Additionally, the optimal cost achieved by the ICDO algorithm is7.58%, 3.51%, 13.29%, and 41.30% lower than that obtained by the same set of algorithms, respectively.

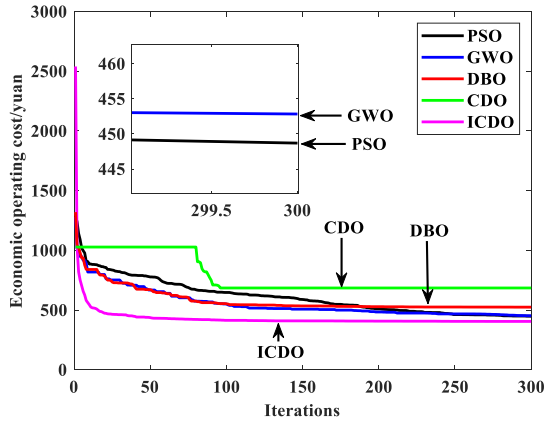

(a) economic operating cost

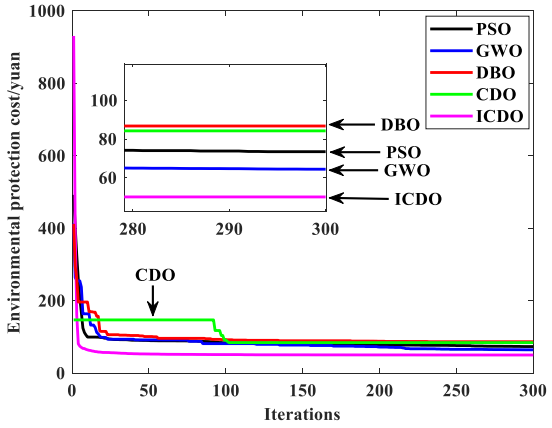

(b) environmental protection cost

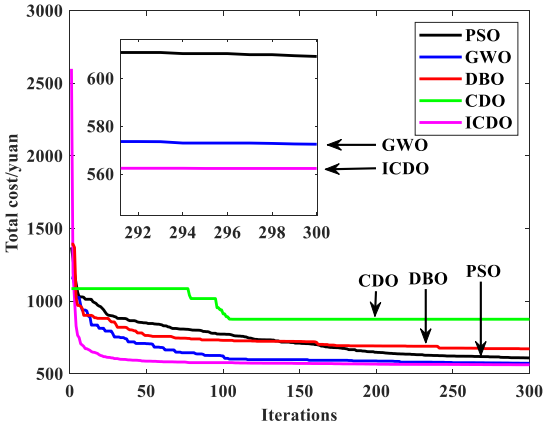

(c) total cost

Fig. 4. The iteration curves under different objective functions

When focusing on minimizing the environmental protection cost, the ICDO algorithm still demonstrates remarkable advantages, with average environmental protection costs reduced by 36.44%, 33.83%, 46.51%, and 56.03%, and optimal environmental protection costs reduced by 30.57%, 24.17%, 35.36%, and 28.59%, compared to the PSO, GWO, DBO, and CDO algorithms, respectively.

When simultaneously considering operating cost and environmental protection cost to minimize the total cost, the ICDO algorithm continues to exhibit its superiority. The average total cost is reduced by 10.95%, 5.66%, 17.55%, and 40.57%, while the optimal total cost is reduced by 6.04%, 1.18%, 4.91%, and 26.88% compared to the PSO, GWO, DBO, and CDO algorithms, respectively. Across different objective functions, the ICDO algorithm demonstrates the smallest standard deviation.

Therefore, when aiming for the lowest operating cost, the optimal solution obtained by the ICDO algorithm sets the operating cost of the microgrid at 387.27 yuan. In the scenario of minimizing environmental protection cost, the ICDO algorithm results in an environmental protection cost of 43.38 yuan for the microgrid. When pursuing the minimization of total cost, the optimized result of the ICDO algorithm determines the total cost of the microgrid to be 541.65 yuan. As illustrated in Figure 4 and Table 8, the improved ICDO algorithm is capable of swiftly locating the global optimal solution, demonstrating faster convergence speed and superior stability.

3) Comparative analysis of the running time of each algorithm

In real-world engineering applications, the computational efficiency of an algorithm is a key indicator of its practicality. Here, the PSO, GWO, DBO, CDO, and ICDO algorithms are each tested through 30 repeated experiments. The execution time of each run is recorded, and the average value, optimal value, and standard deviation are computed for comparative analysis, as presented in Table 9.

As shown in Table 9, under the same conditions of population size, maximum iteration count, and consistent solution models, the runtime of a given algorithm remains generally consistent across different objective functions. However, for the same objective function, different algorithms exhibit certain differences in runtime. Overall, the DBO algorithm has the shortest runtime, indicating higher computational efficiency. The GWO, PSO, and CDO algorithms follow, while the ICDO algorithm has a relatively longer runtime. It is worth noting that although the actual runtime of the ICDO algorithm is marginally longer than that of the CDO algorithm, its theoretical time complexity has not increased, and it offers superior optimization performance and convergence speed. The increase in runtime is mainly due to the additional computational steps introduced by the multi-strategy coordination mechanism (including Tent chaotic mapping, group cognition mechanism, and local search), rather than an escalation in the iteration count or the order of theoretical time complexity.

In summary, the ICDO algorithm demonstrates strong optimization capability and fast convergence while maintaining a reasonable computational cost, significantly outperforming the other comparative optimization algorithms.

(2) Optimization analysis of output power for distributed units in microgrid

This paper performs a comprehensive analysis of the optimal scheduling outcomes derived by the ICDO algorithm in the grid-connected mode of a microgrid. Figure 5 presents

TABLE VIII
COMPARISON OF SIMULATION RESULTS OF FIVE ALGORITHMS UNDER DIFFERENT OBJECTIVE FUNCTIONS

Objective function	Statistical Results	PSO	GWO	DBO	CDO	ICDO
economic operating cost	Average (yuan)	471.66	443.59	523.81	833.88	402.69
	Optimal Value (yuan)	419.03	401.36	446.65	659.76	387.27
	Standard Deviation	24.46	26.82	40.51	95.09	7.26
environmental protection cost	Average (yuan)	69.77	67.01	82.90	100.85	44.34
	Optimal Value (yuan)	62.48	57.21	67.11	71.97	43.38
	Standard Deviation	3.53	4.40	5.91	17.97	0.56
total cost	Average (yuan)	623.68	588.70	673.62	934.55	555.38
	Optimal Value (yuan)	576.46	548.13	569.63	740.80	541.65
	Standard Deviation	21.43	24.17	42.70	85.88	6.92

TABLE IX
COMPARISON OF THE RUNNING TIMES OF FIVE ALGORITHMS UNDER DIFFERENT OBJECTIVE FUNCTIONS

Objective function	algorithm	PSO	GWO	DBO	CDO	ICDO
economic operating cost	Average(s)	2.6084	2.6945	2.2952	2.6987	4.2273
	Optimal Value(s)	2.5125	2.5894	2.2411	2.6496	4.1547
	Standard Deviation	0.0443	0.0347	0.0471	0.0508	0.0777
environmental protection cost	Average(s)	2.6154	2.6848	2.2988	2.6777	4.2313
	Optimal Value(s)	2.4719	2.5377	2.2470	2.6131	4.1379
	Standard Deviation	0.0644	0.0644	0.0390	0.0378	0.0689
total cost	Average(s)	2.5469	2.6541	2.2917	2.7198	4.2053
	Optimal Value(s)	2.4413	2.5206	2.2021	2.5870	4.0695
	Standard Deviation	0.1038	0.1435	0.1086	0.2119	0.1807

the optimal output of each distributed unit under different objective functions.

Figure 5 demonstrates that, for the same microgrid model, different optimal scheduling results are obtained under varying objective functions. Wind and solar energy are clean sources of energy and are therefore given priority in power generation. As illustrated in Figure 5, wind power output is continuous throughout the 24 hours, while photovoltaic power generation, influenced by solar radiation, only occurs from 6 AM to 6 PM, with no photovoltaic generation during other time periods.

Figure 5(a) depicts the optimal output of each distributed generator under the objective of minimizing operating cost. In this case, the generation cost of DE is lower than the microgrid's electricity selling price to the main grid, while the generation cost of MT is higher. As a result, DE operates at full capacity during peak, flat, and off-peak hours, while MT remains idle. The operational cost incurred during charging and discharging of the BESS results in its lower output throughout the scheduling period. To maintain the stability and continuity of power supply, the BESS alternates between charging and discharging to ensure that the initial and final energy levels are equal. During the peak hours from 18:00 to 22:00, as electrical load demand increases significantly, DE alone cannot meet the supply requirements, and the generation cost of MT exceeds the price of buying power from the utility grid for the microgrid. Thus, the microgrid opts to purchase electricity from the main grid during these hours to ensure uninterrupted power supply. In other periods, while satisfying the internal load demand, excess electricity generated by DE is sold to the main grid, creating additional revenue streams and reducing the microgrid's operating costs.

Figure 5(b) presents the optimal output of each distributed generation unit with the objective of minimizing environmental protection costs. In this scenario, MT incurs lower environmental protection costs than purchasing electricity from the main grid, whereas DE has the highest environmental protection costs. Consequently, MT operates at full capacity throughout the scheduling period. Since BESS does not generate environmental protection costs during charging and discharging, and to maintain equal initial and final energy levels, it frequently switches between charging and discharging states, resulting in a more pronounced output compared to Figure 5(a). During peak hours from 18:00 to 22:00, when the electrical load demand soars, MT alone cannot meet the supply, even with additional purchases from the main grid. Consequently, DE is activated to ensure stable and continuous power supply. In other periods, although MT runs continuously, it still cannot satisfy the load demand, thereby necessitating electricity procurement from the main grid. The amount of purchased electricity is influenced by both the load demand and the charging/discharging state of the BESS.

Figure 5(c) demonstrates the optimal output distribution of each distributed generation unit under the objective of minimizing the total cost. During off-peak hours from 1:00 to 7:00 and 23:00 to 24:00, when the load demand is relatively low, MT does not operate. BESS alternates between charging and discharging to provide and reserve electricity. DE's output power is the lowest throughout the scheduling period due to BESS discharging at its maximum output power at 3:00. In other hours, DE operates almost at full capacity. As the electricity selling rate of the microgrid system exceeds the production costs of DE and BESS, there are opportunities to sell power to the main grid for profit. Between 5:00 and 7:00, when the main grid electricity price is low, the microgrid opts to purchase power to charge the BESS, preparing for peak-hour discharging. During flat hours from 8:00 to 9:00 and 16:00 to 17:00, BESS charges during high-demand hours. MT, GRID, and DE remain in similar states as during off-peak periods without significant changes. During peak hours from 10:00 to 15:00, DE operates almost at full capacity, BESS continuously discharges, and sells excess electricity to the main grid, while MT remains idle. From 18:00 to 22:00, influenced by the constraint of equal initial and final energy levels, BESS first discharges and then charges. At 20:00, due to a surge in electrical load, DE alone cannot meet the supply. To ensure reliable and continuous power supply, GRID and MT operate at their maximum output capacity.

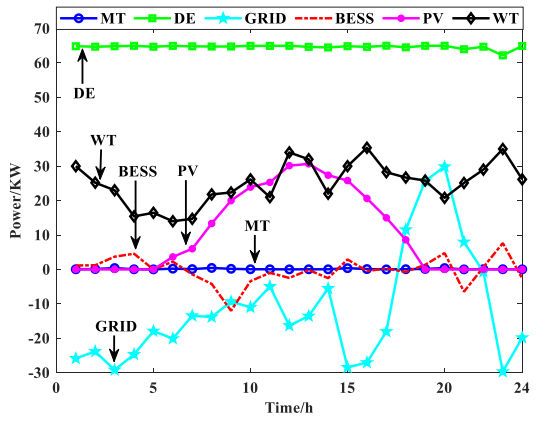

(a) economic operating cost

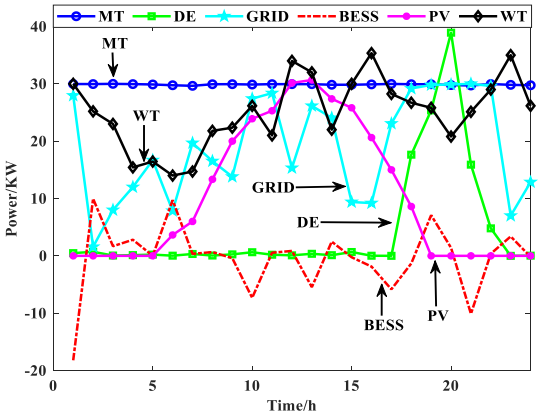

(b) environmental protection cost

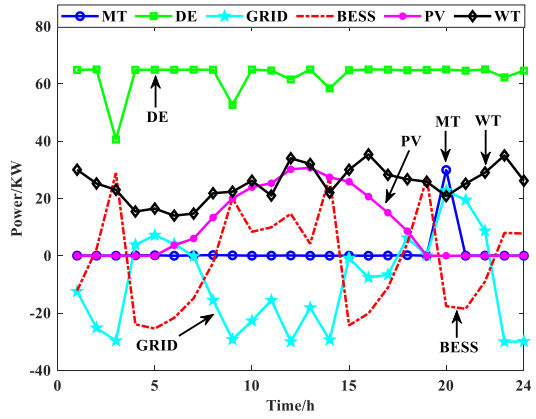

(c) total cost

Fig. 5. Optimal scheduling results of ICDO algorithm under different objective functions

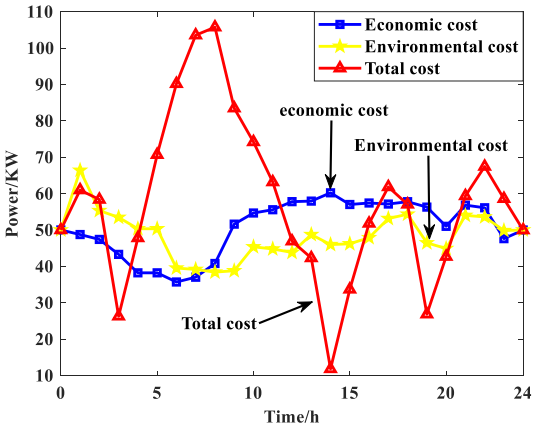

Fig. 6. The curve of battery capacity status changes.

Figure 6 demonstrates the variations in battery capacity states under distinct objective functions.

As shown in Figure 6, regardless of whether the objective function is to minimize operational costs, environmental protection costs, or total costs, the battery's state of charge (SOC) conforms to the upper and lower capacity limits during a 24-hour period. With identical initial and final SOC levels, this ensures no impact on the microgrid's optimal scheduling in subsequent cycles.

VII. Conclusion

This paper takes the minimization of economic operation cost, environmental protection cost, and total cost as optimization objectives, respectively, and establishes an optimal dispatch model for grid-connected microgrids. To achieve these optimization objectives, an improved ICDO algorithm is proposed, which integrates tent chaotic mapping, group cognition mechanism and local search strategy. Through ablation studies, the effectiveness and feasibility of the three improvement strategies are verified. Through the analysis of convergence and optimization accuracy, the superiority of the improved algorithm is proved. In the context of optimal scheduling and grid-connection of microgrids, the enhanced ICDO algorithm is further compared with the four aforementioned algorithms across different objective functions. The results indicate that the ICDO algorithm demonstrates significant advantages in terms of average value, optimal value, and standard deviation. Key insights and conclusions drawn from the paper are as follows:

(1) When economic operating cost are minimized as the objective function, the ICDO algorithm reduces the average cost by 14.62%, 9.22%, 23.12%, and 51.71% respectively compared to the other four algorithms. Similarly, the optimal cost is reduced by 7.58%, 3.51%, 13.29%, and 41.30%.

(2) When environmental protection cost is minimized, the ICDO algorithm exhibits remarkable superiority, lowering the average cost by 36.44%, 33.83%, 46.51%, and 56.03% relative to other algorithms. Accordingly, the optimal cost is decreased by 30.57%, 24.17%, 35.36%, and 28.59%.

(3) When considering total cost, which encompass both operational and environmental protection costs, the ICDO algorithm's advantages remain evident. Compared to PSO, GWO, DBO, and CDO, the ICDO algorithm decreases the average total cost by 10.95%, 5.66%, 17.55%, and 40.57%, respectively, and the optimal total cost is reduced by 6.04%, 1.18%, 4.91%, and 26.88%.

(4) Across various objective functions, the ICDO algorithm exhibits the smallest standard deviation, further attesting to its stability and reliability.

Based on these results, it is clear that the ICDO algorithm exhibits exceptional optimization and solving capabilities within the multi-constraint microgrid grid-connected model, outperforming the PSO, GWO, DBO, and CDO algorithms, even when faced with diverse objective functions. However, it is worth noting that the paper has its limitations. Specifically, when addressing composite benchmark functions, the ICDO algorithm's advantage over the CDO algorithm diminishes. Additionally, the paper's focus has been limited to the economic operating cost, environmental protection costs, and total costs, without exploring other

potential objectives such as power supply reliability and robustness, which could serve as promising avenues for future research.

REFERENCES

[1] X. Wang, S. Chen, Y. Zhou, J. Wang, and Y. Cui, "Optimal dispatch of microgrid with combined heat and power system considering environmental cost," *Energies*, vol. 11, no. 10, p. 2493, Sep. 2018.

[2] M. H. Saeed, W. Fangzong, B. A. Kalwar, and S. Iqbal, "A review on microgrids' challenges & perspectives," *IEEE Access*, vol. 9, p. 166502-166517, Dec. 2021.

[3] F. Rodríguez, A. Fleetwood, A. Galarza, and L. Fontán, "Predicting solar energy generation through artificial neural networks using weather forecasts for microgrid control," *Renewable Energy*, vol. 126, pp. 855-864, Mar. 2018.

[4] Z. Xin, Z. Ze, X. Yi, and M. Jin, "Economic-environmental dispatch of microgrid based on improved quantum particle swarm optimization," *Energy*, vol. 195, p. 117014, Jan. 2020.

[5] M. F. Ishraque, S. A. Shezan, M. M. Ali, and M. M. Rashid, "Optimization of load dispatch strategies for an islanded microgrid connected with renewable energy sources," *Applied Energy*, vol. 292, p. 116879, Apr. 2021.

[6] X. Yang, J. Long, P. Liu, X. Zhang, and X. Liu, "Optimal scheduling of microgrid with distributed power based on water cycle algorithm," *Energies*, vol. 11, no. 9, p. 2381, Sep. 2018.

[7] A. Beirami, V. Vahidinasab, M. Shafie-khah, and J. P. Catalão, "Multiobjective ray optimization algorithm as a solution strategy for solving non-convex problems: A power generation scheduling case paper," *International Journal of Electrical Power & Energy Systems*, vol. 119, p. 105967, Mar. 2020.

[8] S. Roy, S. Goswami, A. Pal, A. Kumar, H. K. Singh, and M. Biswas, "Application of modified particle swarm optimization technique for economic scheduling of a complex micro grid with renewable energy sources" in 2018 2nd International Conference on Trends in Electronics and Informatics (ICOEI). *IEEE*, pp. 77-83, 2018.

[9] Q. Zhang, J. Ding, W. Shen, J. Ma, and G. Li, "Multiobjective particle swarm optimization for microgrids pareto optimization dispatch," *Mathematical Problems in Engineering*, vol. 2020, pp. 1-13, Mar. 2020.

[10] A. Askarzadeh, "A memory-based genetic algorithm for optimization of power generation in a microgrid" *IEEE Transactions On Sustainable Energy*, vol. 9, no. 3, pp. 1081-1089, Dec. 2017.

[11] T. T. Nguyen, T. G. Ngo, T. K. Dao, and T. T. T. Nguyen, "Microgrid operations planning based on improving the flying sparrow search algorithm," *Symmetry*, vol. 14, no. 1, p. 168, Jan. 2022.

[12] T. Mandloi, S. K. Sharma, and S. C. Choube, "The energy management of islanded micro grid system using farmland fertility algorithm" *Energy Sources, Part A: Recovery, Utilization, and Environmental Effects*, vol. 45, no. 2, pp. 5031-5051, Apr. 2023.

[13] M. M. Kamal, I. Asharaf, and E. Fernandez, "Optimal energy scheduling of a standalone rural microgrid for reliable power generation using renewable energy resources,". *Energy Sources, Part A: Recovery, Utilization, and Environmental Effects*, vol. 45, no. 1, pp. 485-504, 2023.

[14] Y. W. Liu, L. L. Li, M. L. Tseng, and M. K. Helmi Ali, "Optimal scheduling of combined cooling, heating, and power microgrid based on a hybrid gray wolf optimizer," Journal of Industrial and Production Engineering, vol. 39, no. 4, pp. 277-292, 2022.

[15] M. Zhang, F. Zhang, and Y. Gao, "The optimal scheduling of microgrid: A research based on a novel whale algorithm," *Energy Reports*, vol. 9, pp. 894-903, 2023.

[16] Z. Belboul, B. Toual, A. Bensalem, C. Ghenai, B. Khan, and S. Kamel, "Techno-economic optimization for isolated hybrid PV/wind/battery/diesel generator microgrid using improved salp swarm algorithm," *Scientific Reports*, vol. 14, no. 1, pp. 2920, 2024.

[17] S. Behera, N. B. Dev Choudhury, and S. Biswas, "Maiden application of the slime mold algorithm for optimal operation of energy management on a microgrid considering demand response program," *SN Computer Science*, vol. 4, no. 5, pp. 491, 2023.

[18] Z. Bektas, M. O. Kayalıca, and G. Kayakutlu, "A hybrid heuristic algorithm for optimal energy scheduling of grid-connected micro grids," *Energy Systems*, vol. 12, pp. 877-893, 2021.

[19] H. A. Shehadeh, "Chernobyl disaster optimizer (CDO): a novel meta-heuristic method for global optimization," *Neural Computing and Applications*, vol. 35, no. 15, pp. 10733-10749, 2023.

[20] A. Ashraf et al., "Papering the impact of initialization for population-based algorithms with low-discrepancy sequences," *Applied Sciences,* vol. 11, no. 17, pp. 8190, 2021.

[21] Y. Zhao and L. Liu, "A bit shift image encryption algorithm based on double chaotic systems," *Entropy*, vol. 23, no. 9, pp. 1127, 2021.

[22] D. Sedighizadeh, E. Masehian, M. Sedighizadeh, and H. Akbaripour, "GEPSO: A new generalized particle swarm optimization algorithm," *Mathematics and Computers in Simulation*, vol. 179, pp. 194-212, 2021.

[23] B. A. S. Emambocus, M. B. Jasser, and A. Amphawan, "An optimized continuous dragonfly algorithm using Hill climbing local search to tackle the low exploitation problem," *IEEE Access*, vol. 10, pp. 95030-95045, 2022.

[24] Yan-e Hou, Wenwen He, Xianyu Zuo, Lanxue Dang, and Hongyu Han, "A Task Scheduling Approach based on Particle Swarm Optimization for the Production of Remote Sensing Products," IAENG International Journal of Computer Science, vol. 50, no.1, pp23-31, 2023.

[25] Asmaa Wahba, Reda El-khoribi, and Shereen Taie, "A New Hybrid Model for Energy Consumption Prediction Based on Grey Wolf Optimization," IAENG International Journal of Computer Science, vol. 49, no.2, pp469-481, 2022

[26] Xu Ji, Qiang Qu, Yu-Long Ren, Jia-Xun Lian, and Tian-Ran Jiang, "Improved DBO Algorithm Incorporating Disorienting Behavior and Dynamic Population Strategy for Engineering Problem Solving," Engineering Letters, vol. 33, no. 1, pp90-103, 2025

[27] L. I. Xingshen et al., "Multi-objective optimization dispatching of microgrid based on improved particle swarm algorithm," *Electric Power Science and Engineering*, vol. 37, no. 3, pp. 1, 2021.

[28] C. Wu, B. Xing, and S. Li, "Hierarchical optimal scheduling of microgrid based on sparrow search algorithm," *Southern Power Grid Technology*, pp. 1-9, Nov. 3, 2023.